

Influence of 2D Versus 3D Modeling on the Fatigue Limit Calculations of Bearing Steels during Rolling Contact Fatigue

Anup S. Pandkar
Researcher

*Department of Mechanical Engineering
West Lafayette, Indiana, 47906, USA*

Bryan Allison
Adjunct Professor

*Department of Mechanical Engineering
Pennsylvania State University Behrend, Erie, Pennsylvania,
16563, USA*

Abstract

Previous analytical/computational studies on the estimation of fatigue limit of bearing steels under Rolling Contact Fatigue (RCF) were based on the concept of absence of micro-plasticity near inclusions. However, these studies were based on 2D models rather than realistic 3D models. In present research, the influence of a simplifying 2D finite element modeling assumption on the accuracy of the predicted fatigue limit has been quantified. The results of this study show that a 2D FE model over-predicts the fatigue limit compared to a 3D model in the case of stiff inclusions, and substantially under-predicts it in the case of compliant inclusions and pores. There-fore, it is suggested that use of 3D modeling should be employed, and extreme care must be taken in interpreting the estimates of fatigue limit obtained from 2D models. On a broader scale, the outcomes of this study highlight key differences between 2D versus 3D modeling when studying complex fatigue failure mechanisms such as RCF.

Keywords: Bearing Steels, Fatigue Limit, Finite Element Analysis, Inclusions, Microstructure, Micro-plasticity, Rolling Contact Fatigue

I. INTRODUCTION

In the past several decades, significant research efforts have been undertaken to extend the bearing fatigue lives as well as to ensure accurate bearing life prediction. In 1948, the ground-breaking work of Lundberg and Palmgren [1], [2] (LP) laid down the foundation for modern bearing life prediction methods based on the well-accepted premise that bearing failures nucleate in the subsurface of a material at the location of maximum orthogonal shear stress [3]–[5]. The LP model parameters were calibrated based on tests conducted on air melted steels which would be considered somewhat “dirty” by modern standards. In the following decades, advancement in material technology and manufacturing processes led the bearing industry to tremendous improvements in bearing design and performance. As a result, the original LP model has also undergone modifications to account for these improvements [6], [7]. A critical change in the bearing life prediction methods came in 1985 when Ioannides and Harris [8] introduced a fatigue limit term in their bearing life prediction model. They drew parallels to rotating bending tests performed on bearing steels and proposed that a fatigue limit (a stress below which a component is expected to have an infinite life) also exists for bearing applications and it should be included in the bearing life prediction models. Although, several research articles [9]–[11] do not support the presence of a fatigue limit in bearing applications, the method proposed by Ioannides and Harris has been adopted into ISO standard 281:2007 [12], which is the present industry standard for bearing life prediction.

Several researchers have undertaken studies to calculate the fatigue limit of bearing materials using experimental and analytical/computational methods [13]–[16]. However, due to the high cost of bearing life testing under low stress conditions analytical/computational methods are preferable compared to experimental methods,. The analytical models proposed so far are based on the assumption of a well lubricated and properly installed bearing, which is expected to fail due to pure material fatigue that initiates in the material’s subsurface in the vicinity of micro-structural features such as inclusions, pores or grain boundaries [3], [5], [17]–[24]. These features introduce inhomogeneities into the material volume and thereby act as local stress risers. The stress concentration is responsible for localized yielding, cyclic micro-plastic strain accumulation, crack nucleation and eventually, material failure. However, if the external loading is such that it does not cause any near-inclusion yielding i.e. micro-plasticity, a material can “theoretically” last for an infinite number of fatigue loading cycles. Based on this, an analytical method to determine the fatigue limit of bearing steels based on the idea of an absence of near-inclusion micro-plasticity using Eshelby tensors has been proposed [13]–[15]. However, this method is limited in its applicability. For example, it is limited to ellipsoidal inclusions which are fully bonded to the matrix. Moreover, these studies did not account for other factors such as the effect of temperature on material properties other than the yield strength. The authors of the current article extended this approach by performing a comprehensive FEA based study to determine the relative criticality of various physical and mechanical parameters/factors on the fatigue limit estimation of bearing steels [25].

All of the previous analytical/computational models discussed [13]–[15], [25] were hinged on the assumption of a two-dimensional (2D) plane strain condition. However, a 2D model cannot capture the influence of curvature of contacting bodies and inclusions in the third dimension. For example, a plane strain assumption applied to spherical inclusions implicitly means that the inclusions are modeled as cylindrical rods of infinite length. Therefore, this assumption is expected to affect the resulting stress-strain fields and hence the predicted fatigue limit of material. In the current study, the results of a 2D plane strain FE model are compared with a more realistic 3D FE model to evaluate the influence of this assumption on the resulting fatigue limit. In addition to the works previously discussed which attempt to estimate the fatigue limit of bearing steels, the assumption of 2D FE modeling is commonly used in computational studies on RCF [20], [26]–[31]. Therefore, the present study not only aims to investigate the influence of underlying 2D modeling assumption from previous work by the authors [25], but also provides insight into the effect of such assumption on the outcome of RCF related studies in general. Such a study becomes especially important when dealing with micro-scale drivers of RCF induced failures such as carbides, material defects and grain boundaries.

In summary, the objective of this FEA based study is to determine the influence of a plane strain modeling assumption on the calculation of fatigue limit of bearing steel. The bearing material considered in the present study is AISI M50 steel. Its mechanical properties are discussed in Section 2. The method used for the calculation of fatigue limit is described in Section 3. Details about the FE model and validation of preliminary results are presented in Sections 4 and 5, respectively. The results are presented in Section 6 followed by the conclusions.

II. MATERIAL INFORMATION

The material considered in the present study is AISI M50 steel. M50 is a medium carbon steel which is commonly used in aerospace bearing applications. Since the objective of this study is to determine the influence of simplifying FEA modeling assumption on the fatigue limit of bearing steels, all the simulations are conducted at a constant temperature of 21°C. In order to explain the concept of fatigue limit calculation and the difference between 2D and 3D models, a single, circular aluminum oxide (Al_2O_3) inclusion with a diameter of 5 μm is considered to be present in the microstructure of M50 steel. The elastic modulus of Al_2O_3 inclusion is $E_{inc} = 375$ GPa, which is stiffer than that of the steel matrix ($E_{steel} = 203$ GPa). In the previous study [25], it was shown that pores and debonded inclusions have the greatest influence on the fatigue limit of bearing steels. Therefore, a pore is also considered for the study. However, little experimental data exists regarding the coefficient of friction at the debonded inclusion/matrix interface or the likelihood of partially debonded inclusions present in the steel matrix. Both of these factors are critical to satisfactorily model and study the influence of debonded inclusions on the fatigue limit. Therefore, debonded inclusions are not considered in the present study. The study is then further extended by including a generic inclusion which is more compliant than the steel matrix i.e. $E_{inc} < E_{steel}$. The yielding and/or cracking of the inclusions is outside the scope of the present study. The mechanical properties of both the steel matrix and different inclusions considered are summarized in Table 1 [32], [33]. Lastly, in order to understand if the shape of inclusions plays any role under 3D conditions, an elliptical inclusion with an aspect ratio of three (15 $\mu m \times 5 \mu m$) aligned parallel to the rolling direction is also considered in this study.

Table - 1
Elastic Properties of M50 Steel Matrix & Various Inclusions

| <i>Material</i> | <i>Elastic Modulus (GPa)</i> | <i>Poisson's Ratio</i> | <i>Shear Yield Strength (MPa)</i> |
|--|------------------------------|------------------------|-----------------------------------|
| <i>M50 steel (matrix)</i> | <i>203</i> | <i>0.3</i> | <i>860</i> |
| <i>Al₂O₃ inclusion</i> | <i>375</i> | <i>0.3</i> | <i>Considered elastic</i> |
| <i>Compliant inclusion</i> | <i>100</i> | <i>0.3</i> | <i>Considered elastic</i> |
| <i>Pore</i> | <i>0</i> | <i>N/A</i> | <i>Considered elastic</i> |

III. FATIGUE LIMIT CALCULATION METHOD

The inclusions present in the microstructure of bearing steels usually act as local stress risers increasing the stress in the surrounding steel matrix. However, if the external load is sufficiently low such that there is no micro-plasticity in the material, one can expect the material to “theoretically” have an infinite life [13], [15], [25]. Based on this concept, the fatigue limit of bearing material can be defined as the global stress level below which no micro-scale yielding i.e. micro-plasticity occurs. The stress component that is generally considered to be the most critical for RCF induced failures is the orthogonal shear stress [3]–[5], [34], [35]. Therefore, the orthogonal shear stress is used as a stress measure to define the bearing fatigue limit in the present study. The fatigue limit is calculated by first calculating the stress concentration factor (K_t) to quantify the extent of stress rise caused by the presence of inclusion in the material subsurface. This is achieved by comparing the global (macro-scale) maximum orthogonal shear stress without an inclusion $(T_o)_{max}$ to the local (micro-scale) maximum orthogonal shear stress with an inclusion $(\tau_o)_{max}$ as,

$$K_t = (\tau_o)_{max} / (T_o)_{max} \tag{1}$$

Once K_t is calculated, the fatigue limit of the bearing steel in shear (T_f) can be determined as the ratio between the microscopic yield strength in shear (τ_y) and the stress concentration factor (K_t) as,

$$T_f = \tau_y / K_t \tag{2}$$

K_t can be calculated via FEA using a two-step process. In the first step, the finite element model is solved with specified boundary conditions, loads, and material properties, but without an inclusion present (termed as global model). From this, the magnitude and location of the maximum macro-scale orthogonal shear stress $((T_o)_{max})$ are determined. In the second step, an inclusion is added

at this critical location and the simulation is re-ran with the exact same boundary conditions, loads, and bulk material properties. From this, the maximum micro-scale orthogonal shear stress $((\tau_o)_{max})$ is determined. By comparing the values of the maximum orthogonal shear stress in the two models (with and without an inclusion), K_t can be calculated using Eq. (1). This value can then be used to calculate the global stress that would be necessary to initiate micro-plasticity by defining the local stress $(\tau_o)_{max}$ as the yield limit of the material (τ_y) using Eq. (2). The global stress, T_f calculated using this method represents the fatigue limit (in shear) for the given steel. This method is used throughout the study to quantify the influence of 2D versus 3D FE modeling on the fatigue limit calculation.

IV. FINITE ELEMENT MODELING

Rolling contact fatigue typically nucleates in the subsurface of the material caused by the Hertzian contact load acting between the rolling elements and the raceway. To simulate a Hertzian contact, a FE model of two rollers pressed together under external loads is used. It was shown in previous study by the authors that static contact model gives a conservative estimate of fatigue limit compared to the rolling contact model [25]. Therefore, for computational efficiency, static contact simulations are performed. Two different FE models are developed to study the effect of 2D versus 3D FE modeling on the calculation of the fatigue limit of bearing steels. Both the models were developed using ANSYS® Mechanical Release 15.0 finite element analysis software which are described in the following paragraphs.

The first FE model developed is a 2D model which simulates the Hertzian contact between two cylindrical rollers. It consists of a 9.5 mm diameter cylindrical rod loaded by a 12.7 mm diameter roller. The 2D plane strain modelling assumption is used along with various symmetries and the resulting model is shown in Fig. 1. The steel matrix in the two rollers are assigned the material properties of M50 steel while the inclusion which is added in the subsurface of the bottom roller is assigned the properties of aluminum oxide i.e. Al_2O_3 .

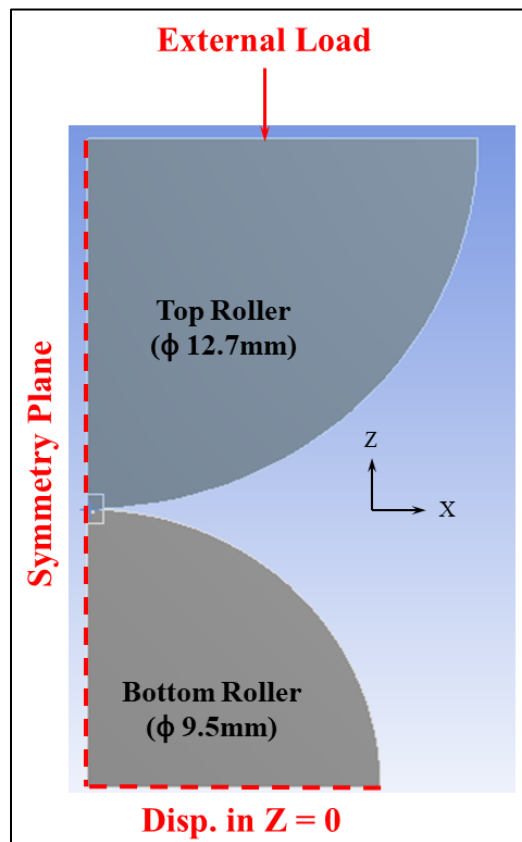


Fig. 1: 2D FE Model Simulating the Hertzian Contact between Two Rollers

As the fatigue limit calculation method is based on the assumption of an absence of micro-plasticity, a linear elastic material model is used for all simulations. A frictionless contact is defined at the contact interfaces between the two rollers. This assumption is considered reasonable as modern bearings are well lubricated with low friction coefficients between the rolling elements and raceways [36]. The external load applied on the top roller is chosen such that it results in a maximum Hertzian contact stress of ~1800 MPa between ball and rod. This value is comparable to typical stress levels experienced by a bearing in service.

The second FE model developed is a 3D model which has the same symmetries as those used for the 2D model. This 3D model is shown in Fig. 2. The length (Y-direction) of each roller is defined to be 4 mm which is significantly larger than both the contact width and the inclusion depth to avoid the influence of edge effects on the stresses in the region of interest.

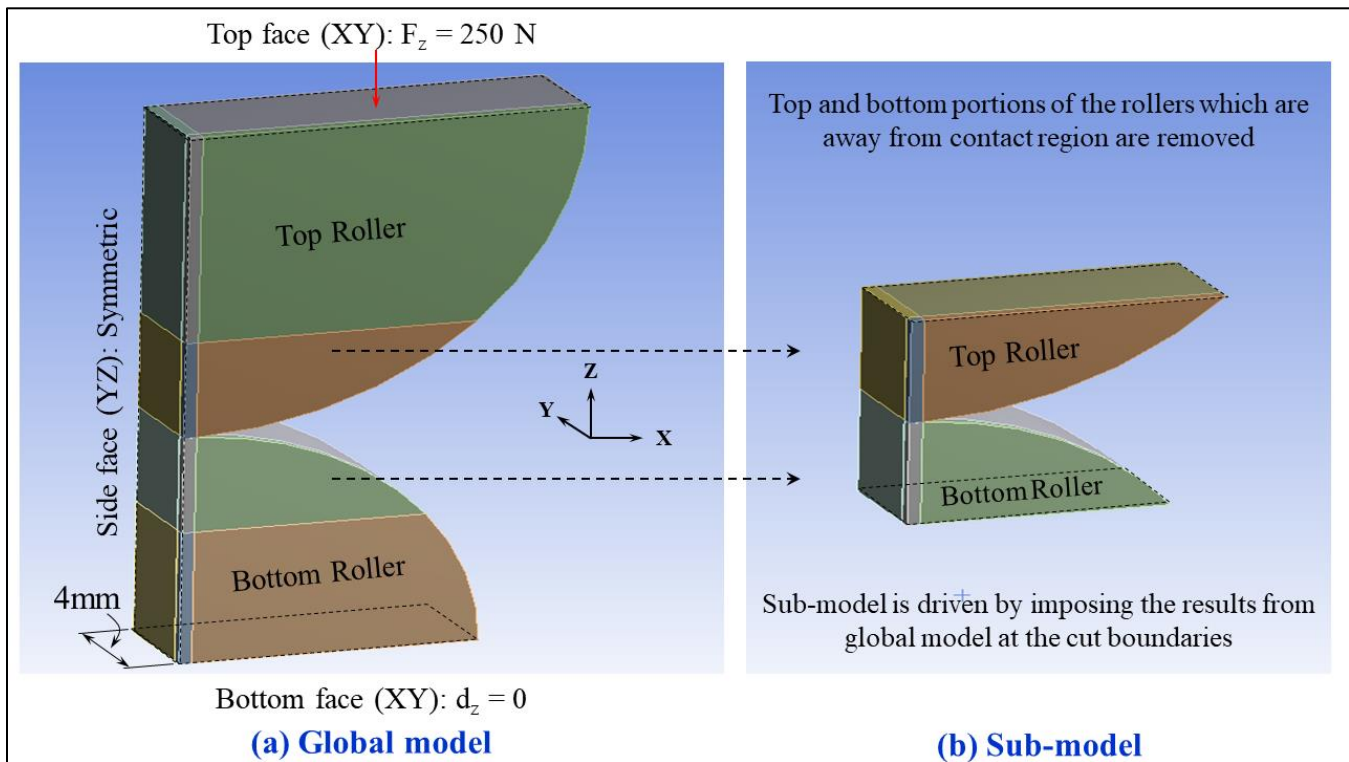


Fig. 2: 3D FE Model Simulating Hertzian Contact between Two Rollers (a) Global Model without Inclusion and (b) Submodel with Inclusion

A force of 250 N was applied on the top face (XY) of the top roller resulting in approximately the same contact pressure of 1800 MPa as used in the 2D model. A submodeling technique was used with the 3D model due to the increased computational expense. In the submodel, the regions away from the contact are removed such that a more refined mesh can be used in the regions of interest (at the contact and in the subsurface) and to ensure convergence. The displacement results obtained from the global model are imposed onto the submodel at the cut boundaries as shown in Fig. 2. As mentioned in Section 3, a two-step finite element modeling approach is used with both the FE models. In the first step, the FE model is ran without any inclusion i.e. global model and the macro-scale maximum orthogonal shear stress ($(T_o)_{max}$) is measured. The critical subsurface location where this maximum occurs is also determined. In the second step, an inclusion is added at this critical location, the models are re-ran, and the micro-scale maximum orthogonal shear stress in the vicinity of this inclusion ($(\tau_o)_{max}$) is measured. For the 3D model, the inclusion is only added into the submodel. Using the macro and micro-scale orthogonal shear stress values, the fatigue limit of material is then calculated following the method explained in Section 3. In both FE models, a well-refined mesh is used in the critical areas (in the vicinity of contact region and inclusions) to ensure mesh convergence and accurate results. It should be noted that in case of 2D plane strain model, a spherical inclusion added to the model gets approximated as a cylindrical inclusion. Whereas, in 3D model, a spherical inclusion gets accurately modeled as spherical which primarily distinguishes the two models and the influence of these modeling choices on the calculation of fatigue limit.

V. VALIDATION OF FE MODELS

The von-Mises and orthogonal shear stress contours obtained from the 2D and 3D global models are shown in Fig. 3. For simple geometries and homogeneous materials without any inclusions, the subsurface Hertzian stresses can be calculated analytically. The theoretical maximum values of contact pressure, von-Mises stress, and orthogonal shear stress were calculated for both 2D and 3D models. These values were then compared to the FEA results of the global models to validate the FE results. A comparison between FEA results and analytical values is summarized in Table 2. The highest discrepancy (error) in Hertzian stress values between the analytical and FEA results is ~2.2% which is considered to be acceptable. Similarly, a well-refined mesh was also used for the FE models with inclusions to ensure convergence.

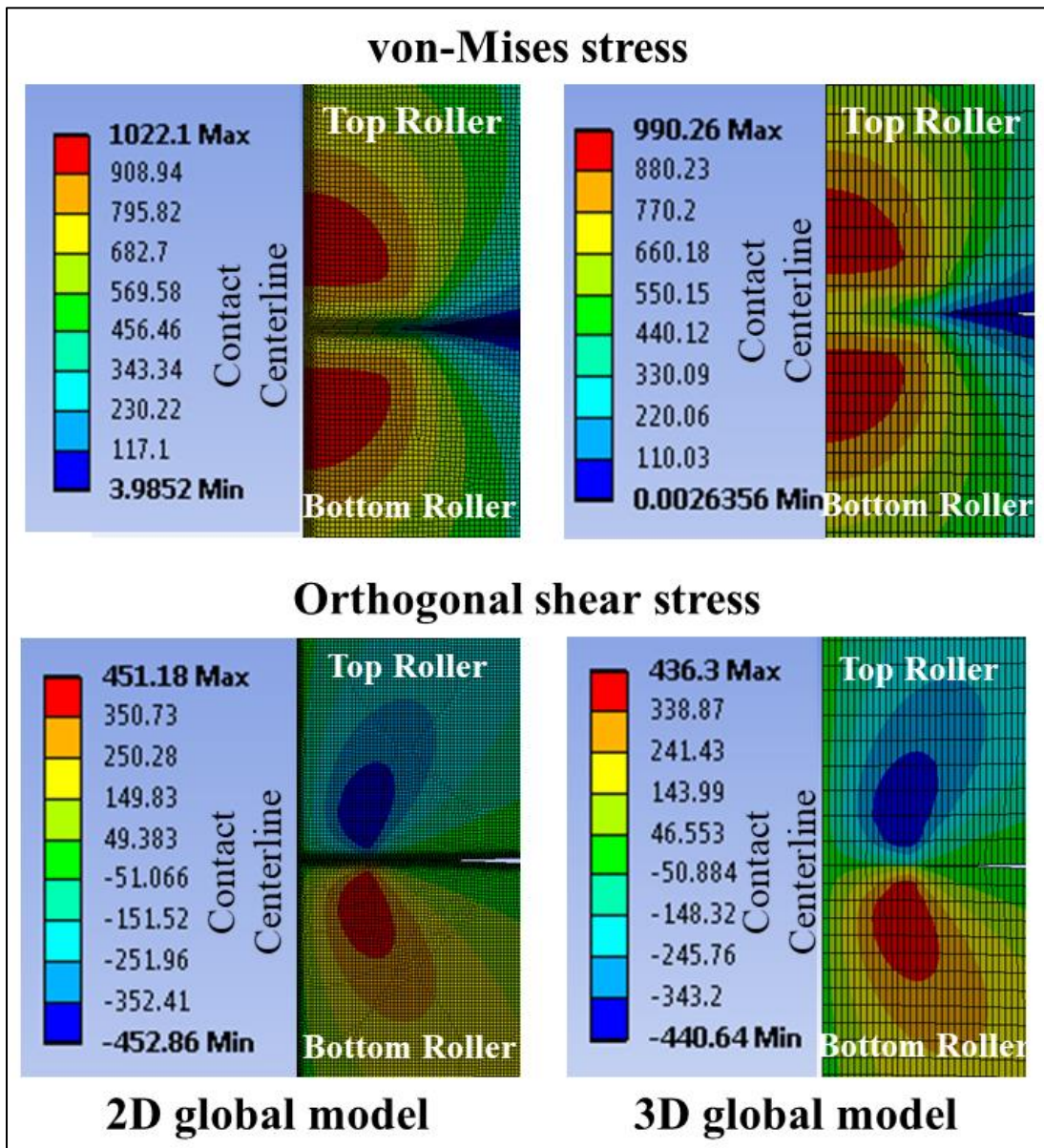


Fig. 3: Von-Mises (top) & Orthogonal Shear (Bottom) Stress Contours for 2D Global (left) & 3D Global Model (Right)

Table – 2
Comparison of theoretical and FEA stress results for the global models without inclusion

| Parameter | Unit | Theoretical value | FE simulation value | | Error (%) | |
|--------------------------------|------|-------------------|---------------------|------|-----------|-----|
| | | | 2D | 3D | 2D | 3D |
| Max. Hertzian contact pressure | MPa | 1800 | 1805 | 1762 | 0.3 | 2.1 |
| Max. von-Mises stress | MPa | 1004 | 1022 | 990 | 1.8 | 1.4 |
| Max. orthogonal shear stress | MPa | 441 | 451 | 436 | 2.2 | 1.1 |
| Max. shear stress | MPa | 540 | 549 | 537 | 1.6 | 0.6 |

VI. RESULTS & DISCUSSIONS

In this section, the results from 2D and 3D FE models (with and without inclusions) are compared to study their effect on the calculation of fatigue limit. The results are first discussed for a circular, 5 μm in diameter, aluminum oxide (Al_2O_3) inclusion, and are then generalized for other inclusions types.

Fig. 4(a) shows the orthogonal shear stress contours in the subsurface of the 2D global model (without an inclusion) and the location at which it occurs is represented by the white circle. Once the magnitude and location of $(T_o)_{max}$ are determined from the global model, an Al_2O_3 inclusion is added in the bottom roller at that location and simulation is re-ran. Fig. 4(b) shows the orthogonal shear stress contours in the vicinity of an inclusion in bottom roller. For better visualization of the stresses in the steel matrix, the inclusion geometry is hidden in Fig. 4(b). Once the maximum orthogonal shear stress values are obtained from FE

simulations, the fatigue limit for the 2D model with Al₂O₃ inclusion can be determined based on the method explained in Section 3. The results from these calculations are summarized in Table 3. Accordingly, the fatigue limit calculated for a 2D FE model in the presence of a circular, 5 μm in diameter, Al₂O₃ inclusion is 683 MPa.

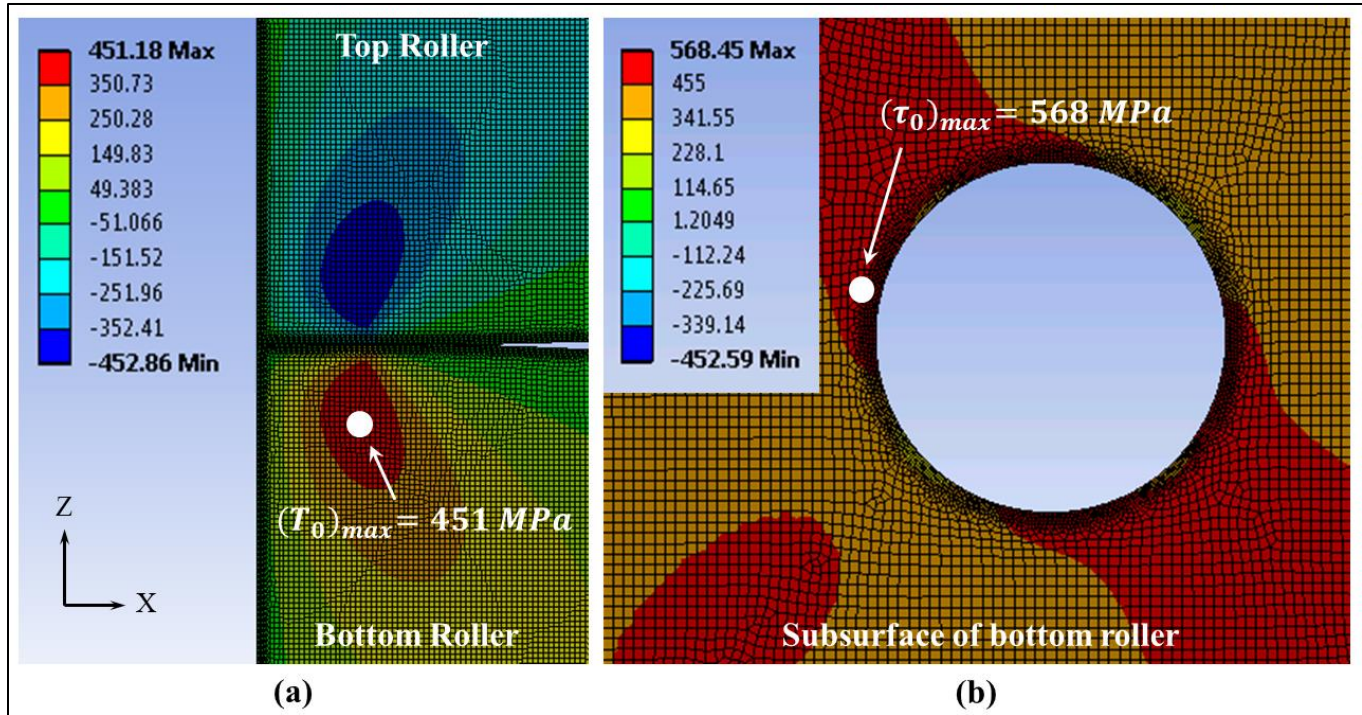


Fig. 4: Orthogonal Shear Stress Contours for 2D FE Model, (a) without Inclusion, (b) with Inclusion (Circular, 5 μm, Al₂O₃)

Table – 3
Calculation of Fatigue Limit using 2D FE model

| Parameter | Notation | Value |
|---|------------------|-------|
| Macro-scale maximum orthogonal shear stress | $(T_o)_{max}$ | 451 |
| Micro-scale maximum orthogonal shear stress | $(\tau_o)_{max}$ | 568 |
| Stress concentration factor | K_t | 1.26 |
| Yield strength in shear | τ_y | 860 |
| Fatigue limit in shear | T_f | 683 |
| * All values are in MPa except for K_t | | |

Similarly, the fatigue limit is then calculated using a 3D FE model in the presence of an identical inclusion. Fig. 5 shows the orthogonal shear stress contours for the 3D FE model with and without an inclusion. For better visualization, the results are plotted in the relevant orthogonal shear stress plane in both figures and the inclusion geometry is hidden to clearly display the stresses in the steel matrix only in Fig. 5(b). The fatigue limit calculation method adopted for 2D model is also used for the 3D model and the results are summarized in Table 4. By comparing the fatigue limit values in Table 3 and Table 4, it is clear that there is approximately 7% discrepancy in the predicted fatigue limit between 2D and 3D FE models. More importantly, the fatigue limit calculated using 3D model is actually seen to be lower compared to the 2D model. This means that the use of plane strain modeling assumption results in a non-conservative estimate of the fatigue limit.

To further explore the effect of 2D versus 3D FE modeling, FE simulations are ran considering a few additional cases. First, an elliptical inclusion with an aspect ratio of three (15 μm x 5 μm in size) with its major axis oriented parallel to the rolling direction is considered. In addition, the material properties assigned to the inclusion are replaced with 1) a compliant inclusion with ($E_{inc} = 100$ GPa) and, 2) a pore ($E_{inc} = 0$ GPa).

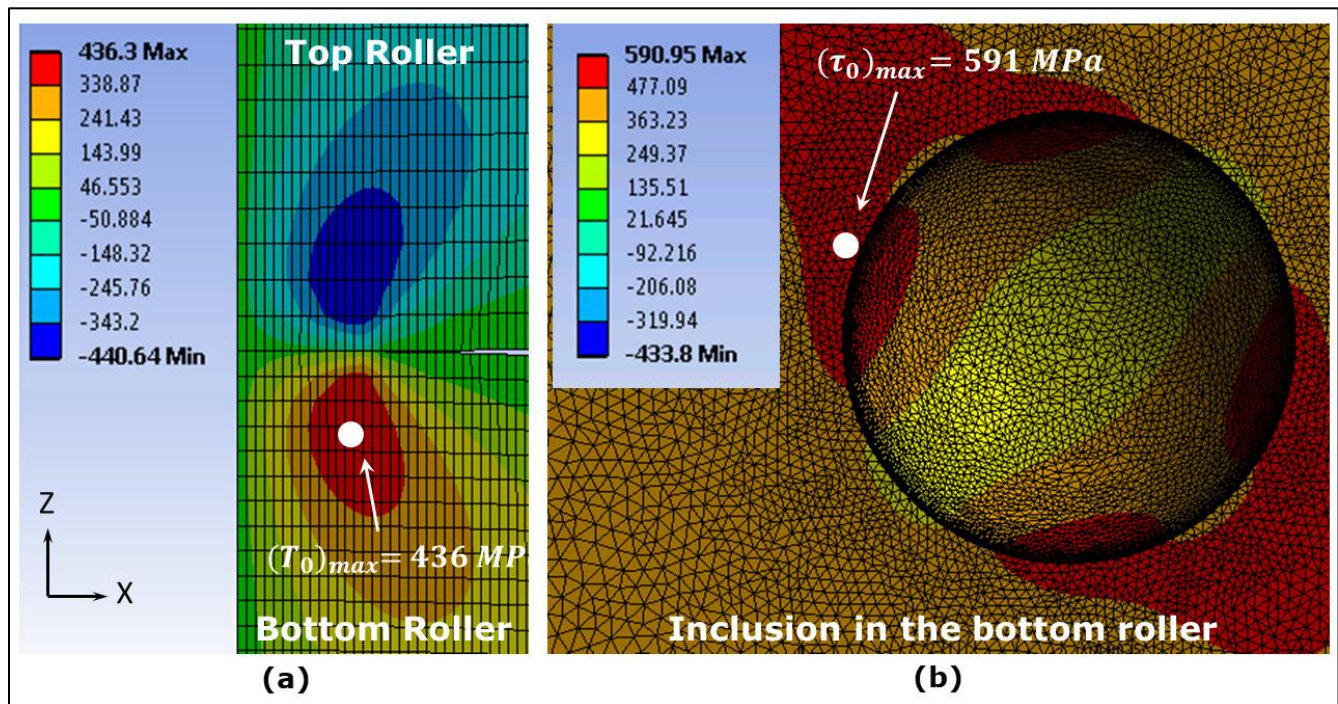


Fig. 5: Orthogonal Shear Stress Contours for 3D FE Model, (a) without Inclusion, (b) with Inclusion (Spherical, 5 μm , Al_2O_3)

Table – 4
Calculation of Fatigue Limit using 3D FE Model

| Parameter | Notation | Value |
|---|------------------|-------|
| Macro-scale maximum orthogonal shear stress | $(T_0)_{max}$ | 436 |
| Micro-scale maximum orthogonal shear stress | $(\tau_0)_{max}$ | 591 |
| Stress concentration factor | K_f | 1.35 |
| Yield strength in shear | τ_y | 860 |
| Fatigue limit in shear | T_f | 637 |
| * All values are in MPa except for K_t | | |

For the combination of elliptical/circular inclusion and stiff/compliant/pore inclusions, five additional simulations are ran and fatigue limit is calculated for each case. The results are summarized in Table 5, in which the last column represents the ratio of the fatigue limit calculated using 2D and 3D FE models. The results of this can be visualized in Fig. 6.

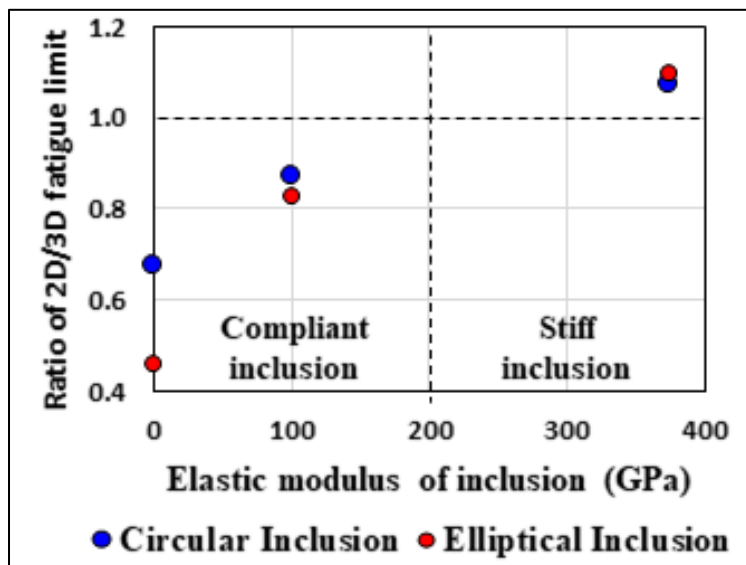


Fig. 6: Relative comparison of Fatigue Limit Values for Different Inclusion Geometries and Stiffnesses

Based on these calculations, following important conclusions can be drawn. First, the ratio between the 2D and 3D fatigue limit values is greater than unity when the inclusion is stiffer than the surrounding steel matrix ($E_{inc} > E_{steel}$) regardless of the inclusion geometry. Therefore, use of a 2D FE model (i.e. plane strain assumption) may be a dangerous assumption as it over-predicts the fatigue limit of a material. In contrast, in the case of porosity (or compliant inclusions with $E_{inc} < E_{steel}$), the fatigue limit calculated using 2D FE models is significantly lower than for the 3D FE models. Therefore, when dealing with porosity (or compliant inclusions) care must be taken as the calculated fatigue limit might be significantly under-predicted (although it will be a conservative estimate). And lastly, the qualitative prediction of the fatigue limit is not affected by the shape of inclusion i.e. for a given inclusion stiffness, both circular and elliptical inclusions show similar trends of over/under prediction of the fatigue limit with 3D models.

Table – 5
Comparison of 2D versus 3D Fatigue Limit Values for Inclusions with Different Geometries and Stiffnesses

| Type of inclusion | Fatigue Limit (MPa) | | |
|---|---------------------|----------|---------------|
| | 2D model | 3D model | Ratio = 2D/3D |
| Stiff circular ($E_{inc} = 375$ GPa) | 682 | 635 | 1.07 |
| Stiff elliptical ($E_{inc} = 375$ GPa) | 710 | 646 | 1.10 |
| Compliant circular ($E_{inc} = 100$ GPa) | 512 | 588 | 0.87 |
| Compliant elliptical ($E_{inc} = 100$ GPa) | 475 | 576 | 0.83 |
| Circular pore ($E_{inc} = 0$ GPa) | 248 | 367 | 0.68 |
| Elliptical pore ($E_{inc} = 0$ GPa) | 152 | 332 | 0.46 |

VII. CONCLUSIONS

Previous analytical and computational studies on the fatigue limit of bearing steels were based on the idea of absence of micro-plasticity in the subsurface. However, these studies were based on the use of plane strain models instead of more realistic 3D models. In this manuscript, the effect of this assumption on the resulting fatigue limit was quantified for different inclusion geometries and stiffnesses. Overall, it was found that the use a plane strain assumption led to a significant difference in the predicted fatigue limit. It was found that in the presence of stiff inclusions ($E_{inc} > E_{steel}$), a plane strain assumption results in over-prediction of the fatigue limit. In contrast, when compliant inclusions (including pores) are considered, a plane strain assumption results in conservative estimates of the fatigue limit, but with a high discrepancy. Based on these results, it is recommended that 3D models be used for future estimation of the fatigue limit of bearing steels. If a 2D model is used, care must be taken in interpreting/using the estimated fatigue limit values. In addition to specific conclusions pertaining to calculation of fatigue limit, this study also shows that Hertzian stress distribution in the subsurface of material is sensitive to the choice of 2D versus 3D finite element modeling employed. Since this choice directly affects the stress distribution in the vicinity of inclusions, the fatigue damage predictions associated with any rolling contact fatigue related study will be significantly affected by this choice. As a result, the decision to use 2D or 3D modeling should be made carefully. In general, 2D modeling can be used in qualitative studies and 3D modeling should be used when quantitative results of simulation are more important.

NOMENCLATURE

- E_{inc} : Elastic modulus of inclusion
- E_{steel} : Elastic modulus of steel matrix
- K_t : Stress concentration factor
- $(T_o)_{max}$: Macro-scale max. orthogonal shear stress
- $(\tau_o)_{max}$: Micro-scale max. orthogonal shear stress
- T_f : Fatigue limit of material in shear
- τ_y : Microscopic shear yield strength

REFERENCES

- [1] G. Lundberg, "Dynamic capacity of rolling bearings," IVA Handlingar, vol. 196, p. 50, 1947.
- [2] G. Lundberg and A. Palmgren, "Dynamic Capacity of Rolling Bearings," Acta Polytechnica, Mechanical Engineering Series, vol. 2, no. 4, 1952.
- [3] T. A. Harris and M. N. Kotzalas, Essential concepts of bearing technology. CRC press, 2006.
- [4] T. A. Harris and M. N. Kotzalas, Advanced concepts of bearing technology: rolling bearing analysis. CRC Press, 2006.
- [5] F. Sadeghi, B. Jalalahmadi, T. S. Slack, N. Raje, and N. K. Arakere, "A Review of Rolling Contact Fatigue," Journal of Tribology, vol. 131, no. 4, p. 41403, 2009.
- [6] American Society of Mechanical Engineers and E. N. Bamberger, Life adjustment factors for ball and roller bearings; an engineering design guide. New York: American Society of Mechanical Engineers, 1971.
- [7] E. V. Zaretsky, "STLE life factors for rolling bearings," STLE SPECIAL PUBLICATION SP, 1992.
- [8] E. Ioannides and T. A. Harris, "A New Fatigue Life Model for Rolling Bearings," Journal of Tribology, vol. 107, no. 3, pp. 367–377, 1985.
- [9] E. V. Zaretsky, "In search of a fatigue limit: A critique of ISO Standard 281:2007," Tribology and Lubrication Technology, vol. 66, pp. 33–40, 2010.
- [10] S. Shimizu, "Fatigue Limit Concept and Life Prediction Model for Rolling Contact Machine Elements," Tribology Transactions, vol. 45, no. 1, pp. 39–46, Jan. 2002.

- [11] C. Sakae and L. M. Keer, "Application of direct method for a nonlinear-kinematic-hardening material under rolling/sliding line contact: constant ratcheting rate," *Journal of the Mechanics and Physics of Solids*, vol. 45, no. 9, pp. 1577–1594, 1997.
- [12] "ISO Standard 281:2007, Rolling Bearings - Dynamic Load Ratings and Rating Life," 2007.
- [13] P. Lamagnere et al., "A Physically Based Model for Endurance Limit of Bearing Steels," *Journal of Tribology*, vol. 120, no. 3, pp. 421–426, Jul. 1998.
- [14] A. Vincent, R. Fougères, G. Lormand, G. Dudragne, and D. Girodin, "A Physically Based Endurance Limit Model for Through Hardened and Surface Hardened Bearing Steels," in *Bearing Steel Technology*, ASTM International, 2002.
- [15] J. Courbon, G. Lormand, G. Dudragne, P. Daguier, and A. Vincent, "Influence of inclusion pairs, clusters and stringers on the lower bound of the endurance limit of bearing steels," *Tribology international*, vol. 36, no. 12, pp. 921–928, 2003.
- [16] T. A. Harris, "Establishment of a New Rolling Bearing Fatigue Life Calculation Method," Final Report US Navy Contract, no. 00421, pp. 93–124, 2002.
- [17] P. C. Becker, "Microstructural changes around non-metallic inclusions caused by rolling-contact fatigue of ball-bearing steels," *Metals Technology*, vol. 8, no. 1, pp. 234–243, Jan. 1981.
- [18] A. M. Kumar, G. T. Hahn, and C. A. Rubin, "A study of subsurface crack initiation produced by rolling contact fatigue," *Metallurgical and Materials Transactions A*, vol. 24, no. 2, pp. 351–359, 1993.
- [19] A. S. Pandkar, A Microstructure Sensitive Study of Rolling Contact Fatigue in Bearing Steels. [electronic resource] A Numerical and Experimental Approach. [Gainesville, Fla.] : University of Florida, 2014.
- [20] A. S. Pandkar, N. Arakere, and G. Subhash, "Ratcheting-based microstructure-sensitive modeling of the cyclic hardening response of case-hardened bearing steels subject to Rolling Contact Fatigue," *International Journal of Fatigue*, vol. 73, pp. 119–131, Apr. 2015.
- [21] H. Singh, R. V. Pulikollu, W. Hawkins, and G. Smith, "Investigation of Microstructural Alterations in Low- and High-Speed Intermediate-Stage Wind Turbine Gearbox Bearings," *Tribology Letters*, vol. 65, no. 3, p. 81, May 2017.
- [22] N. Hoa Ngan and P. Bocher, "Finite Element Analysis Simulation of the Effect of Induction Hardening on Rolling Contact Fatigue," *Journal of Tribology*, vol. 140, no. 6, pp. 061404-061404–10, Jul. 2018.
- [23] K. C. Mutyala, H. Singh, J. A. Fouts, R. D. Evans, and G. L. Doll, "Influence of MoS₂ on the Rolling Contact Performance of Bearing Steels in Boundary Lubrication: A Different Approach," *Tribology Letters*, vol. 61, no. 2, p. 20, Jan. 2016.
- [24] A. Bhattacharyya, A. Pandkar, G. Subhash, and N. Arakere, "Cyclic Constitutive Response and Effective S–N Diagram of M50 NiL Case-Hardened Bearing Steel Subjected to Rolling Contact Fatigue," *Journal of Tribology*, vol. 137, no. 4, pp. 041102–041102–15, Oct. 2015.
- [25] B. Allison and A. Pandkar, "Critical factors for determining a first estimate of fatigue limit of bearing steels under rolling contact fatigue," *International Journal of Fatigue*, vol. 117, pp. 396–406, Dec. 2018.
- [26] V. Bhargava, G. T. Hahn, and C. A. Rubin, "Analysis of rolling contact with kinematic hardening for rail steel properties," *Wear*, vol. 122, no. 3, pp. 267–283, Mar. 1988.
- [27] E. Kabo, "Material defects in rolling contact fatigue — influence of overloads and defect clusters," *International Journal of Fatigue*, vol. 24, no. 8, pp. 887–894, 2002.
- [28] E. Kabo and A. Ekberg, "Material defects in rolling contact fatigue of railway wheels—the influence of defect size," *Contact Mechanics and Wear of Rail/Wheel Systems*, vol. 258, no. 7–8, pp. 1194–1200, 2005.
- [29] N. Raje, F. Sadeghi, J. Rateick Richard G., and M. Hoerich, "Evaluation of Stresses Around Inclusions in Hertzian Contacts Using the Discrete Element Method," *Journal of Tribology*, vol. 129, no. 2, pp. 283–291, 2007.
- [30] A. A. Walvekar and F. Sadeghi, "Rolling contact fatigue of case carburized steels," *International Journal of Fatigue*, vol. 95, pp. 264–281, Feb. 2017.
- [31] W. Wang, H. Liu, C. Zhu, P. Bocher, H. Liu, and Z. Sun, "Evaluation of Rolling Contact Fatigue of a Carburized Wind Turbine Gear Considering the Residual Stress and Hardness Gradient," *Journal of Tribology*, vol. 140, no. 6, pp. 061401-061401–10, May 2018.
- [32] "Latrobe Lescalloy® M50 VIM-VAR High Performance Bearing Steel [WWW Document], 2008, Last accessed," Mar. 2018.
- [33] Y. S. Touloukian, "Thermophysical Properties of High Temperature Solid Materials. Volume 4. Oxides and Their Solutions and Mixtures. Part 1. Simple Oxygen compounds and Their Mixtures," *Thermophysical and Electronic Properties Information Analysis Center, Lafayette, IN*, 1966.
- [34] S. Suresh, *Fatigue of Materials*, 2nd Edition, ISBN: 978-0-521-57847-9, Cambridge University Press., 1998.
- [35] A. S. Pandkar, N. Arakere, and G. Subhash, "Microstructure-sensitive accumulation of plastic strain due to ratcheting in bearing steels subject to Rolling Contact Fatigue," *International Journal of Fatigue*, vol. 63, pp. 191–202, Jun. 2014.
- [36] D. Glover, "A ball-rod rolling contact fatigue tester," *ASTM STP*, vol. 771, pp. 107–125, 1982.